www.czasopisma.pan.pl PAN www.journals.pan.pl
Opto-Electronics Review 26 (2018) 122–133

Contents lists available at ScienceDirect

Opto-Electronics Review

journal homepage: http://www.journals.elsevier.com/opto-electronics review

Review Invited

Selected optoelectronic sensors in medical applications

Z. Bielecki [a,*], T. Stacewicz [b], J. Wojtas [a], J. Mikołajczyk [a], D. Szabra [a], A. Prokopiuk [a]

[a] Institute of Optoelectronics, Military University of Technology, gen. Witolda 2 Urbanowicza Str., Warsaw 00-908, Poland
[b] Institute of Experimental Physics, Faculty of Physics, University of Warsaw, 5 Pasteura St., Warsaw 04-093, Poland

ARTICLE INFO

Article history:
Received 24 January 2018
Received in revised form 26 February 2018
Accepted 28 February 2018
Available online 25 April 2018

Keywords:
Optoelectronic sensors
Medical sensors
Invasive sensors
Non-invasive sensors
MUPASS
CEAS
Breath analyses
Medical screening

ABSTRACT

Optoelectronic technology plays an important role in medical diagnosis. In the paper a review of some optoelectronic sensors for invasive and non-invasive human health test is presented. The main attention is paid on their basic operation principle and medical usefulness. The paper presents also own research related to developing of tools for human breath analysis. Breath sample unit and three gaseous biomarkers analyzer employing laser absorption spectroscopy designed for clinical diagnostics were described. The analyzer is equipped with sensors for CO, CH_4 and NO detection. The sensors operate using multi-pass spectroscopy with wavelength modulation method (MUPASS-WMS) and cavity enhanced spectroscopy (CEAS).

Contents

1. Introduction

Optoelectronic sensors (OS) are applied in many life and scientific activities, e. g.: environmental monitoring, industry, chemical analysis, biology, and medicine. Current medical applications of OS include pulse oximetry, heartrate monitoring, measuring the amount of oxygen in the blood, blood glucose monitoring, urine analysis, dental colour matching, and exhaled biomarkers monitoring. These sensors must meet strict requirements, they should be safe, biocompatible, reliable, stable, suitable for sterilization, immune for biologic rejection and miniaturized. Maintaining of these devices should be as simple as possible.

Idea of the OS operation bases on analyses of light-matter interactions. Main processes which occur in the matter illuminated by

* Corresponding author.
E-mail address: zbigniew.bielecki@wat.edu.pl (Z. Bielecki).

https://doi.org/10.1016/j.opelre.2018.02.007
1230-3402/

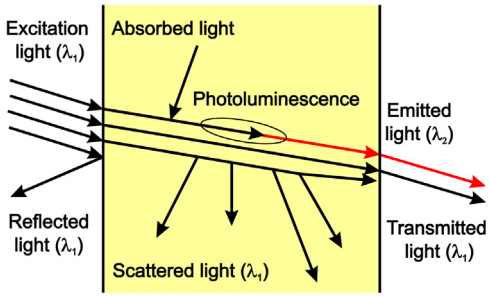

Fig. 1. Some phenomena caused by the light-matter interaction [1].

radiation at a given wavelength λ_1 are schematically shown in Fig. 1.

The nature of the interaction depends on specific features of the matter. The result of the interaction can be used as matter signature (marker). For example, scattered light is used for liquid investigation (blood flow monitoring or glucose detection). Substances characterization (identification) by analysis of their specific absorption spectrum is of high significance for medical measurements. OS based on absorption usually quantify the change in intensity and spectrum of light that is transmitted through the sample. Reflectance sensors are also designed for such specific analysis but for the substances of low transparency. When excited molecule of the sample returns to the ground singlet state S_0, it can emit photons at longer wavelength range than the absorbed one (Fig. 2). The absorbed radiation can also cause *fluorescence* at wavelength different than λ_1 (λ_2 in Fig. 1). Due to internal conversion the molecule can also return to the S_0 state via triplet state T_1 in case of *phosphorescence* phenomenon. This effect lasts longer than fluorescence, and produces lower energy radiation (longer wavelength). For both cases, the emission intensity is proportional to concentration of excited molecules.

Parameters measured commonly in medical diagnosis can be divided into physical and chemical ones (Table 1). Since stimuli are not electrical, there is several energy conversion steps in the medical sensor before it produces an electrical signal, that is measured and interpreted as representing the parameter of interest. In case of the OS, photon flux is always detected by a photodetector providing a conversion into the electric signal. For example, a periodic stress acting on a fiber-optic pressure sensor, first results in strain in the fiber, which causes a change of its refractive index and change of optical transmission, which finally results in modulation of the photon flux registered by a photodiode.

Table 1
Selected medical parameters [3].

Physical parameters	Chemical parameters
Pressure	Bilirubin concentration
Temperature	pH
Blood flow	Oxygen partial pressure
Humidity	Carbon dioxide partial pressure
Cataract onset	Lipoproteins
Radiation dose	Lipids
Biting force	

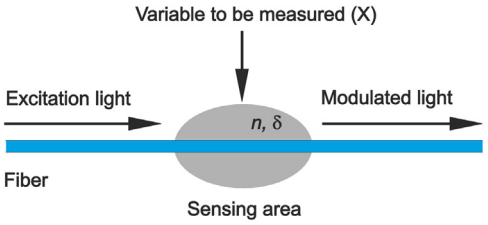

Fig. 3. Idea of operation optical fiber intrinsic sensor.

In fiber-optic OS, the light may be directly modulated either by the parameter being investigated and acting on the fiber or by special reagent connected to the fiber. The optical properties of the reagent vary with the change in the stimulation agent of measured medium. Such a probe is often called an optrode. Fluorescence, absorption, Raman scattering, evanescent-wave and plasmon resonance are the main physical phenomena of its operation. The simplest fiber OSs classification is based on the subdivision in *intrinsic* and *extrinsic sensors*.

In intrinsic sensors (Fig. 3), the fiber plays a role of a light guider and transducer. In this case, the investigated substance modifies refraction index (n) or losses coefficient (δ) of the fiber. Then the

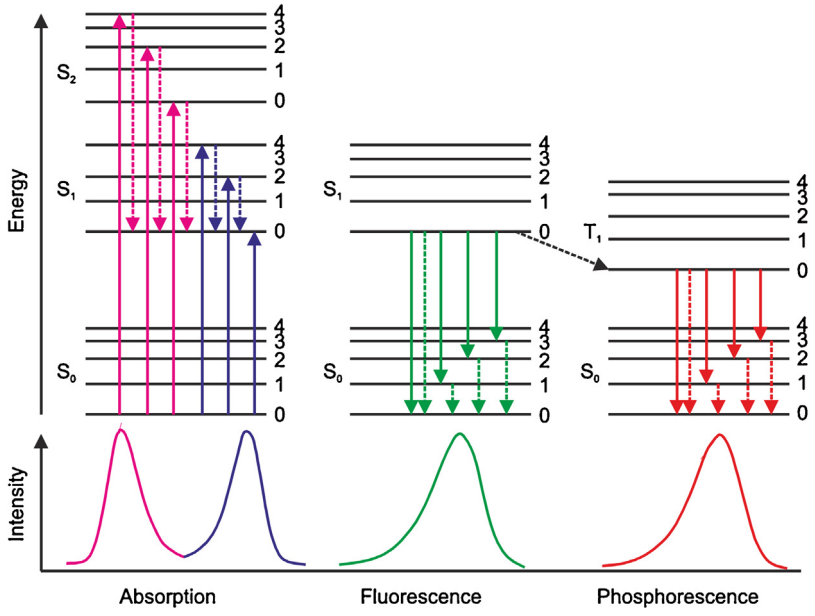

Fig. 2. Jablonski diagram representing energy levels and spectra. Solid arrows indicate radiative transitions as occurring by absorption (violet, blue) or emission of a photon [2].

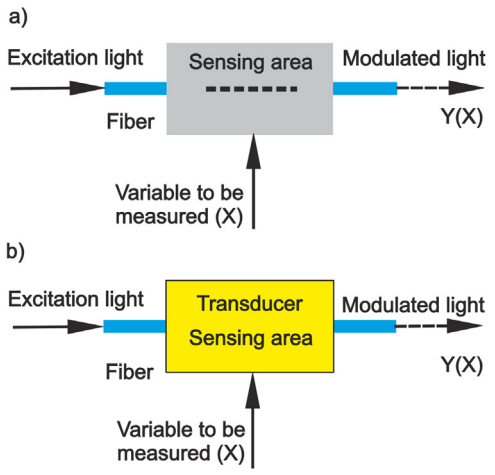

Fig. 4. Idea of operation optical fiber extrinsic sensor.

radiation transmitted in the fiber will vary depending on the substance quantity [4].

Extrinsic sensors use the optical fiber to guide the light from the source to sensing area (outside the fiber) where a light modulation takes place. The modulation can concern various light parameters such as intensity, wavelength, polarization angle, phase, or time delay [1]. Next, modulated light is collected and transmitted through the fiber to photodetector [Fig. 4a)]. The investigated substance produces direct modulation of the light or acts on a transducer, which finally cause the change in light parameters [Fig. 4b)].

Light intensity monitoring is the simplest solution for most of OS. However, its measurement is sensible to changes in light source parameters, fiber couplings, fiber attenuation, signal noises, etc. These factors reduce accuracy of the measurement. Therefore, such interferometric configuration as Sagnac, Michelson, Mach-Zehnder and Fabry-Perot are used for error minimizing [5].

The medical test can be carried out on a living organism (in vivo) or outside the body (in vitro). Furthermore, taking into account the sample testing procedure, the medical sensors can be divided into [6]:

- non-invasive sensors, in which the probe remains outside of human body or on the skin surface (contacting),
- minimally invasive (indwelling),
- invasive sensors, in which the probe must enter the human body through the nostrils, throat, butthole, ears, or implantable.

In the next sections we shall briefly discuss the principles and ideas of invasive and noninvasive optoelectronic sensors used in medicine. The first group included: endoscopic imaging, bile sensor, pH meter, oxygen and carbon dioxide sensors, cardiac and pressure sensors. Following examples are shown as non-invasive devices: pulse oximeter, blood flow-meter, glucose meter, sensor of prostate cancer, optical coherence tomography and human breath analyzers. We will also take a brief look at the results of our research related to development ultrasensitive gas sensors, which can be applied in human breath analyzing and clinical screening.

2. Invasive optical sensors in medicine – selected examples

2.1. Endoscopic imaging

Development of flexible fibers has facilitated manufacturing of many modern medical devices, e.g.: *endoscopic imaging systems* [7]. Fig. 5 shows a system design of a video endoscopy. Such instruments comprise a light source, optical fiber, CCD unit, image processing unit, and instrument channel. The endoscope fiber transmits light from a source into the body, illuminating the cavity where the endoscope has been inserted. Light reflected off the body part travels back to CCD unit, and electrical signal is sent to an image processing unit for various kinds of image enhancement. Endoscopy is used for examination of the gastrointestinal tract, for confirmation of a diagnosis, most commonly by performing a biopsy, as well as to check the conditions such as bleeding, inflammation, clipping off a polyp or control of foreign object removing.

2.2. Bile sensor

Optical fiber sensor plays also important role in detection of enterogastric and non-acid gastroesophageal refluxes [8]. The operation principle of the bile-containing reflux sensor is based on the detection of the presence of bilirubin, the main biliary pigment. The sensor consists of a probe, light emitting sources and signal-processing unit (Fig. 6).

The miniaturized probe supplies the light into the stomach or the esophagus and conducts the back signals to the photodiode [9–11]. Two LEDs operating at 465 nm and 570 nm are used as the radiation sources. First wavelength is matched to the characteristic absorption band of bilirubin and the second is utilized as reference

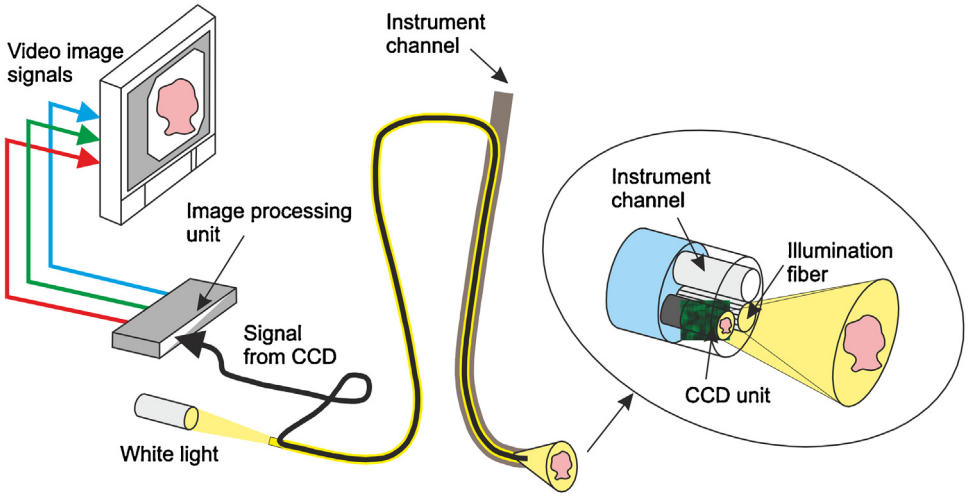

Fig. 5. Simplified scheme of video endoscopy system.

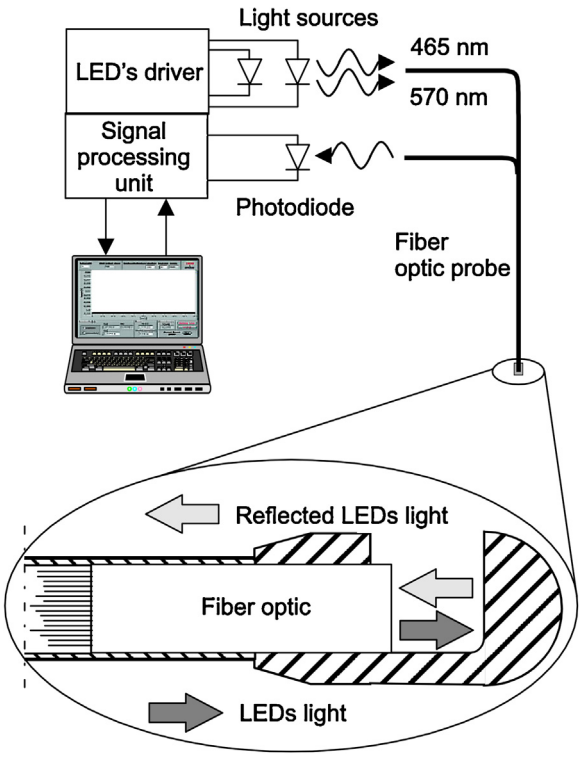

Fig. 6. Block diagram of the fiber optics bile sensor.

[8]. Their light, scattered by digestive matter system, is registered and elaborated by the signal processing unit that calculates the difference in the absorbancies at these wavelengths. This difference value is proportional to the bilirubin concentration that is related to bile reflux. Sensor sensitivity is about 2.5 μmol/l [8].

2.3. *pH, oxygen and carbon dioxide optical sensors*

Potential of hydrogen ion (pH) monitoring is very important, because it is related to diagnosis of the many organs in human body. pH-value of various body fluids, such as blood, urine, saliva or gastric acid is measured. Optical pH sensors exploit pH indicator dyes, which are typically weak organic acids or bases with their protonated (acidic) and deprotonated (basic) forms [12]. These indicators interact with hydrogen ion H_3O^+ and test the change of their optical properties, such as absorption, fluorescence or reflectance as a

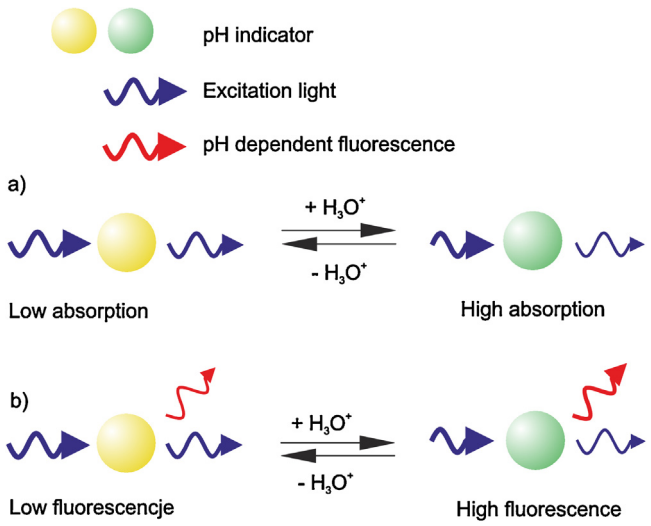

Fig. 7. Schematic representation of absorption (a) and fluorescence-based pH sensing mechanism (b) [15].

function of the environment pH [13]. A schematic representation of absorption and fluorescence based sensing is shown in Fig. 7. Some fiber-optic pH OS's are based on evanescent-wave principles [14].

Such sensors can be used for real-time pH monitoring of the blood, detection of activity in stomach and in esophagus. Current practice consists in insertion of a miniaturized probe in the stomach or the esophagus through the nostrils.

Fig. 8 shows schemes of the pH optrode, similar to bile sensor. The sensor consists of two channels: channel 1 (pH range 1–3.5) and channel 2 (pH range 3.5–8). Each channel is built of two LEDs (one for the signal and the other for the reference) and a photodiode.

All range of interest (1–8 pH units) requires use of two dyes: bromophenol blue – BPB and thymol blue – TB. The chromophores are deposited at the end of optical fibers (sensitive layer). Emission wavelengths of LEDs were chosen on the basis of the optical properties of the chromophore: 565 nm (signal) and 830 nm (reference) for channel 1, and 605 nm (signal) and 830 nm (reference) for channel 2. The signals coming from the probe are amplified and processed by an optoelectronic unit [16]. A teflon diffuse reflector is applied in order to improve the return coupling of the scattered light.

Simultaneously with pH monitoring, oxygen and carbon dioxide diagnostics is very useful for many fields of medicine. Content of

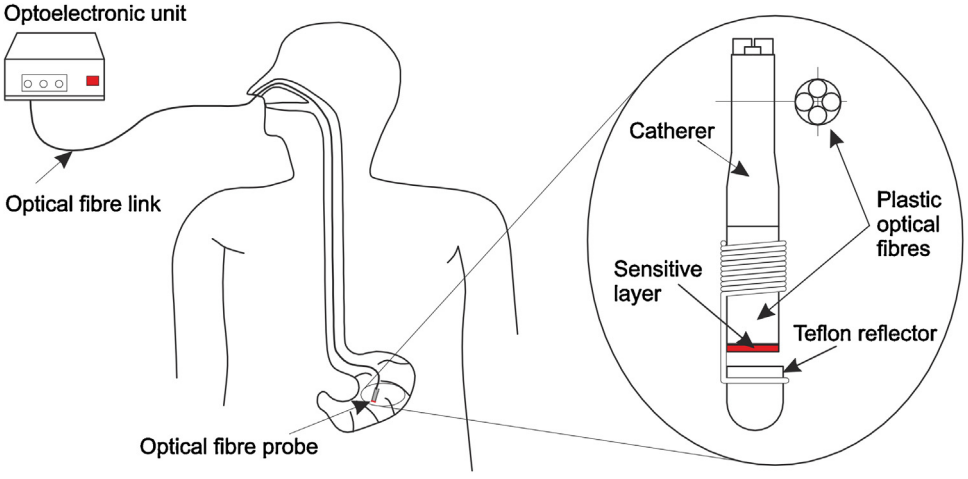

Fig. 8. Schemes of OS in the stomach monitoring and of pH optical probe.

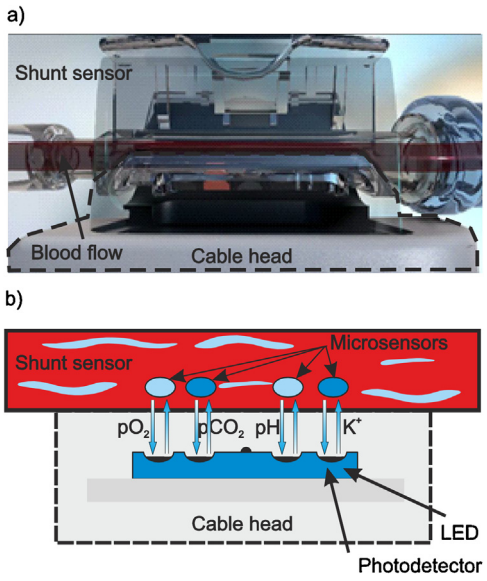

Fig. 9. Optical fluorescence sensor [18].

oxygen in blood is an essential indicator for cardiovascular and cardiopulmonary systems diagnosis, while the gastric carbon dioxide monitoring can help in rating of the disturbances in tissue perfusion. Real time knowledge about oxygen and carbon dioxide partial pressures in surgery rooms or intensive-care units (pCO_2, pO_2) is crucial for determination of oxygen quantity delivered to the tissues.

Based on optical fluorescence and reflectance technologies the CDI Blood Parameter Monitoring System 500 measures or calculates 11 critical blood parameter values, including: pH, pCO_2, pO_2, potassium (K^+) and other [17].

Fig. 9a) shows one of the main components of the system, shunt sensor, which is applied to measure pH, pCO_2, pO_2 and K+ in arterial or venous blood. The shunt sensor is placed in a shunt line where blood is in direct contact with system's sterile microsensors [Fig. 9b)]. The sensor contains four microsensors and a thermistor. LEDs mounted in the cable heads irradiate the microsensors, which contain fluorescent dyes. As a result a fluorescent light is emitted from the microsensors surfaces. A photodetector in the cable head detects this light. Its intensity, which is proportional to the concentration of the medium of interests, is displayed on the monitor screen.

The intensity value depends on pH, pCO_2, pO_2, and K+ presence in the blood, and is used for their monitoring [18]. The pH, pCO_2, pO_2 measurements are taken every second, but K+ measurement is taken every six seconds.

2.4. Cardiac monitoring by FBG sensors

A Fiber Bragg Grating (FBG) sensors are used for cardiac monitoring and estimating the stroke volume, blood temperature or heart muscle activity. They are also applied as a laser-ablation delivery probe during the treatment of atrial fibrillation. Its operations consists in a periodical modulation of the refractive index in an optical fiber. When light propagates through a fiber with FBG, a reflection occurs, but only for a narrow wavelength range. For other wavelengths the transmission does not change (Fig. 10).

Central wavelength λ_B of the Bragg band can be expressed:

$$\lambda_B = 2 \cdot n_{eff} \cdot \Lambda, \tag{1}$$

where n_{eff} is the effective refractive index of the fiber core, and Λ denotes the spatial period of the grating. As far as both the spatial period Λ and the refractive index n_{eff} are sensitive for strain and temperature, the technique is implemented for monitoring of these parameters. The wavelength λ_B can be measured by conventional wavemeter. Typical strain sensitivities are 0.64 pm/$\mu\varepsilon$ (where $\mu\varepsilon$ denotes the microstrain – 10^{-6}) while for the temperature – 6.8 pm/°C for λ_B near 830 nm [5].

2.5. Interferometry based fiber optic pressure sensors

Interferometers are widely used for measurement of small displacements, refractive index changes and surface irregularities. In medical applications, the interferometric OSs are mainly dedicated for monitoring of force and pressure (e.g., arterial, intra-tracheal, intracranial and intravascular pressure) [20]. They are important tools in construction of artificial heart [21,22]. An interesting application is related to the intra-aortic balloon pumping therapy which is often used to help patients' recovery from critical heart diseases, as well as in cardiac surgery or to wait until a transplant is performed.

In these devices light is split into two beams which travel different optical paths – the sensing fiber and the reference one (Fig. 11). After interaction with a measurand the light is mixed in a combiner with the signal transmitted by reference fiber. This signal is not affected by tested parameter. As a result, the interference occurs which modulates the light intensity registered by the photodetector.

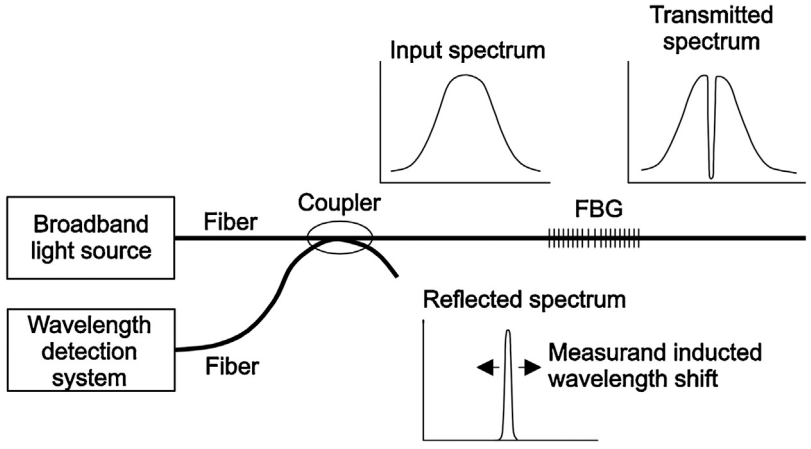

Fig. 10. Operation idea of the FBG sensor [19].

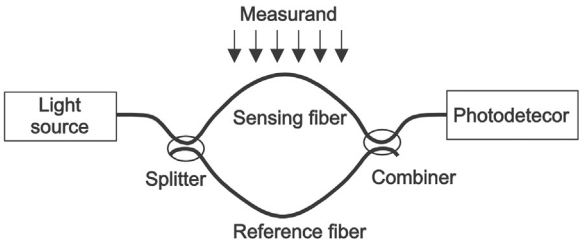

Fig. 11. A fiber optic Mach-Zehnder interferometer.

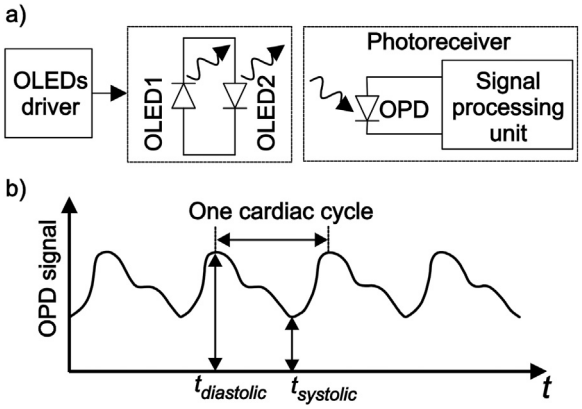

Fig. 12. Pulse oximetry sensor (a) and example of the output signal (b).

The expression of the interferometric signal can be given by:

$$V = V_0(1 + k\cos\varphi), \tag{2}$$

where V_0 is the signal amplitude from the light source, k is the interferometer constant ($0 < k < 1$) and φ is the phase shift at the output due to the propagation path length difference between the sensing fiber ($L_S n_{effS}$) and the reference fiber ($L_R n_{effR}$):

$$\Delta\varphi = 2\pi/\lambda \cdot (L_S n_{effS} - L_R n_{effR}), \tag{3}$$

where λ is the light wavelength.

The interferometer can be used for monitoring of physical parameters affecting the fiber length or its refraction coefficient. Such a fiber-optic OS's can be designed as intrinsic sensors, where the sensing element is the fiber itself, or as extrinsic sensors with a small size sensing element (transducer) attached at the tip of an optical fiber. The detection limit depends largely on the transducer design.

Another type of fiber-optic interferometer which can be used for medical applications is the Fabry-Perot configuration. The optical fiber is coupled to a small optical resonator allowing miniaturization of the measurement system. The system consists of a light source, a photodetector and the resonator providing sample investigation. The compact size of this setup enables direct insertion of the sensing element into the body in clinical procedures.

3. Non-invasive sensors in medicine

3.1. Pulse oximetry

Pulse oximetry is a non-invasive medical sensing method to measure human pulse rate and arterial blood oxygenation. Typical pulse oximeter is composed of two light-sources with different peak emission wavelengths and a single photodiode [Fig. 12a)]. Lochner et al. [23] presented a pulse oximeter sensor based on organic materials, which are compatible with flexible substrates. The sensor is composed of flexible organic polymer photodiode (OPD) and two organic light-emitting diodes (OLEDs): green (532 nm) and red (626 nm). OLEDs light is attenuated by pulsating arterial blood, non-pulsating arterial blood, venous blood and other tissue [Fig. 12b)]. Light quenching depends on the heart's phase (contraction or relaxation). This continuous change in arterial blood volume provides information about the pulse rate and it is represented by AC component of OPD signal. The attenuation of the incident radiation results from absorption of the oxygenated and deoxygenated hemoglobin. Detailed information about this sensor operation is given in few papers [23].

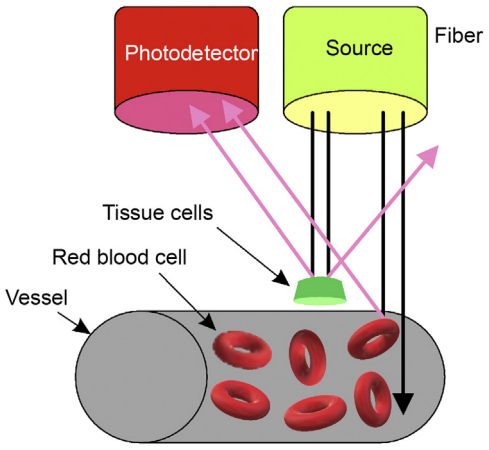

Fig. 13. Idea of fiber-optic laser Doppler flowmeter [25].

3.2. Blood flow-meter

Laser Doppler flowmeter (LDF) is an optoelectronic instrument to record semi-quantitatively pulpal blood flow. The idea of fiber-optic LDF is shown in Fig. 13. Laser light is guided by an optical fiber probe to the tissue or vascular network where it is diffusely scattered and partially absorbed by the investigated sample. The light scattered by moving red blood cells is frequency-shifted. That process depends on the cells velocity and direction of the incident light, whilst those from the static tissue remain unshifted in frequency. The photodetector registers the interference pattern arising from the mixing of shifted and unshifted light (optical heterodyne detection). Blood flow measurement is carried out basing on this signal [24].

In this technique the particle size must be enough large to sufficiently scatter the light for signal detection but also small enough to accurately monitor the flow, i.e. the size should be 1–20 μm [26]. A helium–neon laser (632.8 nm) or diodes lasers (780–820 nm) with the radiation power of about 1 mW are used as the light sources [27].

The use of fiber optics in LDF sensors allows both invasive and non-contact monitoring of very low flow rates, such as blood flow in capillaries, renal blood flow, gingival blood flow, monitoring of skin blood flow rate, blood flow in the optical nerve, etc.

3.3. Blood glucose monitoring

Photoacoustic spectroscopy (PAS) is a very sensitive technique for investigations of gases, liquids and solids. It was also applied to glucose measurements.

Fig. 14 shows a PAS sensor setup designed for glucose measurement. It consists of quantum cascade laser (QCL), flipping mirror (*FM*), lenses (*L1*, *L2*), iris (*I*), laser diode (*DL*) for setup alignment, chopper (*Chop*), power meter (*PM*), *PA* cell with microphone (*Mic*) and humidity-temperature sensor (*RH-T*). Preamplifier, lock-In amplifier and PC are used for signal acquisition. Emission from

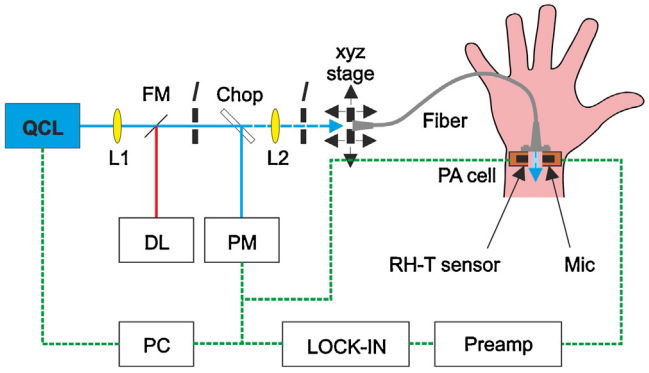

Fig. 14. Scheme of the setup of photoacoustic sensor used for glucose measurement [28].

the external-cavity quantum cascade laser covers the wavelength from 1010 to 1095 cm^{-1}. This includes two strong glucose absorption peaks at 1034 and 1080 cm^{-1}. Detection limit of 140 mg/dl and 57 mg/dl (using SNR = 1 criterion) was reported applying an integration time of 1 s and 45 s, respectively [28].

Ergin et al. [29] described non-invasive techniques for glucose concentration determining in blood by acquisition of Raman spectrum of the aqueous eye lymph. The advantage of this technique is that each metabolite and the eye structure are characterized by an unique Raman spectrum. Therefore the presence of other metabolites in aqueous and other eye structures can be identified. The setup (Fig. 15) consists of a laser (785 nm), optical fiber probe for both excitation and collection, spectrometer and PC for data acquisition and processing. In the system, laser radiation is focused on the sample. The incident light interacts with matter and the wavelength shift is observed [30].

Raman spectroscopy is a very promising tool also for other medical applications. It is characterized by good sensitivity to subtle changes in the chemical and structural characteristics of biological specimens [31–34].

3.4. Microcantilever sensor of prostate cancer

Wu et al. demonstrated microcantilever sensor for cancer diagnosis [35]. In this sensor the surface of the microcantilever with antibodies specific to prostate specific antigen (PSA) is applied. Such marker was found in the blood of patients having prostate cancer. Fig. 16 shows operation idea of a microcantilever-based sensor. This idea is quite simple, however development is highly demanding. Surface of each cantilever is coated with a selective compounds providing analytes adsorption. This mass deposition causes a stress, and leads to a detectable bending of the cantilever. The more analytes is adsorbed, the greater bend is registered using optoelectronic technique. The angular deflection of respective laser beams at the bending surface is processed

3.5. Optical coherence tomography

Optical coherence tomography (OCT) was first reported by Huang et al. in 1991. Team of inventors has been recently awarded by the 2017 Fritz J. and Dolores H. Russ Prize [36]. So far, the method has become an important clinical imaging modality. Thanks to numerous advantages, OCT rapidly transited from research and development into the clinical setting. It offers high quality images (with 0.5 μm resolution) [37], requires the low light fluence level and can be used in sensitive tissue locales, such as the eye [38]. Probes are typically optical fiber-based, and e.g.: they can operate within the gastrointestinal tracts [39]. Furthermore, such type of imaging method is able to render depth-resolved structural images of the target. More sophisticated OCT imaging strategies can provide additional functional information such as flow (through Doppler OCT) or tissue structures [40,41]. Animal studies have also confirmed the imaging of the brain and mammalian embryos [42,43].

The operating principle of OCT can be compared to ultrasound tomography imaging. The beam of pulsed light towards a tissue sample, and like in the case of ultrasound tomography, reflections (echoes backscattered) from the tissue are expected. Basing on time gating and the reflections train, depth-resolved line profile of the tissue can be determined. A two-dimensional depth-resolved image of the sample is obtained by repeating the process at incremental steps across the tissue sample. The reflected pulse train is indirectly measured by interferometry (Fig. 17). In conventional approach, which is time domain OCT (TDOCT), the input light source is split at the beam splitter (BS). One component is directed at the sample, and the other is sent to a movable reference mirror (MM). The backscattered and back reflected light are then re-channeled and combined through the beam splitter and detected by a photodetector (PD). A typical spectrometer-based SDOCT (spectral domain OCT) scheme is very similar to that of a typical TDOCT scheme. The moving reference mirror is immobilized (IM), and the detector is replaced by a low-loss spectrometer in the SDOCT scheme [44]. A Fourier transform of the spectral measurement produces a line scan profile similar to that obtained from TDOCT. SDOCT systems are more sensitive than TDOCT systems, because they are capable of collecting the signals from all depth of the sample during the entire acquisition time [45].

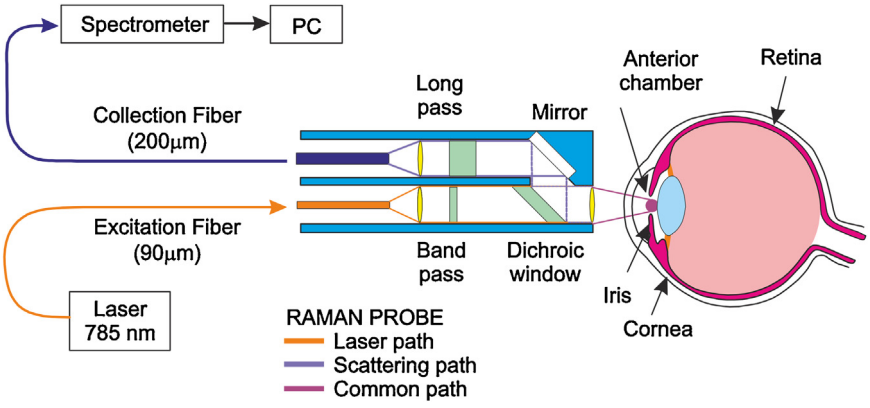

Fig. 15. Scheme of the system setup for noninvasive measurement of glucose [29].

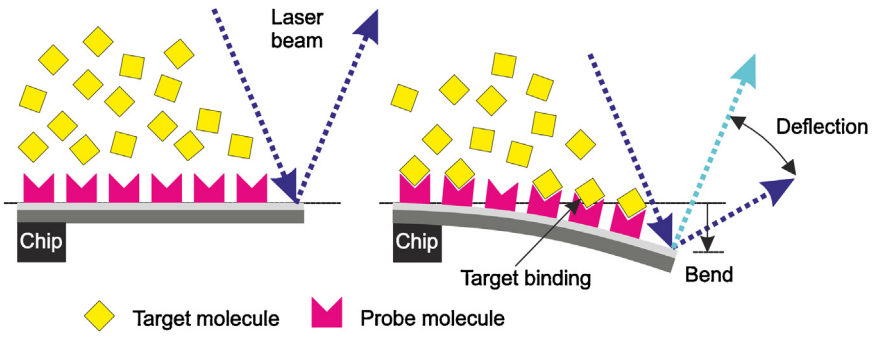

Fig. 16. Operation principle of a microcantilever-based sensor.

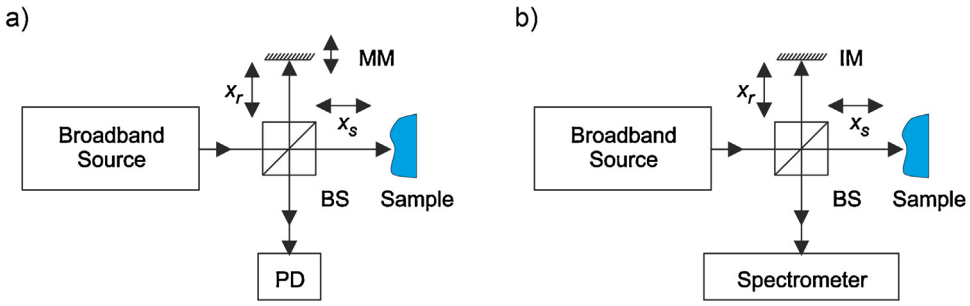

Fig. 17. Simplified schemes of time domain (a) and spectral domain optical coherence tomography systems (b).

4. Human breath analyzers – based on own works

Metabolic processes occurring within the human body create a wide variety of volatile organic compounds (VOCs) in the exhaled air. About 3000 various compounds were already detected. Nitrogen, carbon dioxide, oxygen, water, argon and other products of metabolic processes within the body are the main components of the exhaled air [46]. VOCs are related to a person's diet, stress level and immune status. Compounds like acetone, ethane, pentane and isoprene are known in the medical practice and provide valuable information about the state of a patient's health [47]. In Table 2, some disease biomarkers are listed.

In order to detect gaseous biomarkers in human breath, various methods were developed in the past two decades. The most versatile are gas chromatography combined with mass spectrometry and ion mobility spectrometry [48,49]. Other techniques like chemiluminescence [49], proton transfer reaction mass spectrometry [50], selected ion flow tube mass spectrometry [51], electrochemical sensing or the electronic noses [52], and fiber optoelectronic sensing, are also widely used for this purpose.

Progress in optoelectronic technologies opens capabilities of biomarkers detection by laser absorption spectroscopy (LAS). LAS sensors are characterized by a very high sensitivity and selectivity. They provide opportunity to detect and measure the concentration of specific gases in the sampling place (so–called in situ) or to investigate the samples collected in tedlar bags and transported to the sensor. Here, multi–pass spectroscopy (MUPASS) and cavity enhanced absorption spectroscopy (CEAS) are applied. Their operation idea has been described by Authors in previous publications [47,53]. In MUPASS (Fig. 18) the high sensitivity is achieved due to light path lengthening in the experimental cell containing the investigated gas sample. The cell is equipped with two mirrors. Laser beam is multiply reflected among them passing many times through the sample.

To improve the selectivity and enlarge the immunity of the detection process to noises and interferences, wavelength modulation spectroscopy (WMS) was implemented. It consists in

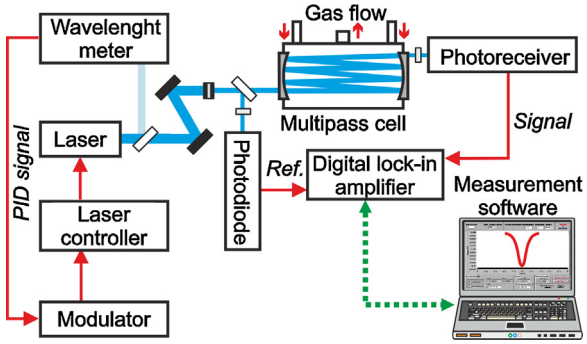

Fig. 18. Setup of MUPASS sensor.

periodical variation of the laser wavelength within the absorption line profile.[1] The relevant periodical changes occur in the photodetector output signal which is then demodulated with a lock–in amplifier. Using both MUPASS and WM the absorption sensitivities of 10^{-7} cm^{-1} (and even better) are available. The scheme of our experimental setup exploiting this method is presented in Fig. 18. In CEAS system, pulsed laser beam is injected at a very small angle versus the optical cavity (resonator) characterized by a high Q-factor (Fig. 19). After each reflection, a small part of laser radiation leaves the cavity due to the residual transmission of the mirrors, and is registered by a photoreceiver. The amplitude of single-mode radiation trapped within the resonator decays exponentially with time. The decay constant characterizes the cavity Q-factor. When the resonator is filled with the analyzed gas absorbing the radiation, Q-factor of the cavity decreases and the decay constant is smaller.

The absorber concentration is proportional to difference between the inversed decay constants for cavity with the absorber and for the case when it is empty.

[1] Using of WMS is more effective in the case of spectroscopy or the matter characterized by narrower absorption lines.

Table 2
Examples of gaseous biomarkers concentration in human breath.

Compound	Normal concentration in exhaled air [ppb]	Physiological source of molecules/Disease	References
Acetone	390–850	Decarboxylation of acetoacetate, diabetes, occurs in breath of children who are on a high-fat diet for the treatment of epilepsy, oxidation of fatty acids, cardiac index.	[54,55]
Ammonia	250–2900	Protein metabolism, liver and renal disease, Helicobacter Pyroli, oral cavity disease.	[56–58]
Carbon monoxide	<10 000	Production catalyzed by heme oxygenase, hyperbilirubina, oxidative stress, respiratory infections, and asthma.	[59–61]
Carbonyl sulfide	0.003–30	Gut bacteria, liver disease, cystic fibrosis, acute rejection of transplanted lungs.	[62–64]
Ethane	~0.12	Lipid peroxidation, vitamin E deficiency, chronic respiratory diseases, cells oxidative stress, an indicator of scleroderma and cystic fibrosis.	[65–68]
Methane	3000–8000	Gut bacteria, colonic fermentation and intestinal problems.	[69,70]
Nitric oxide	50 for adults 35 for children	Production catalyzed by NO synthase, asthma, hypertension, rhinitis and various air way inflammation.	[71–73]
Nitrous oxide	50–200	Synthesis of enzymes	[74–76]

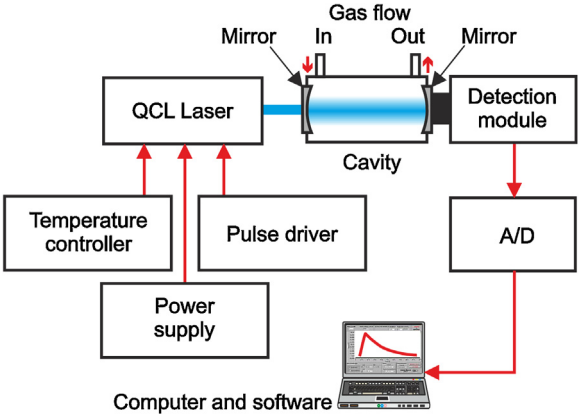

Fig. 19. The scheme of the CEAS setup.

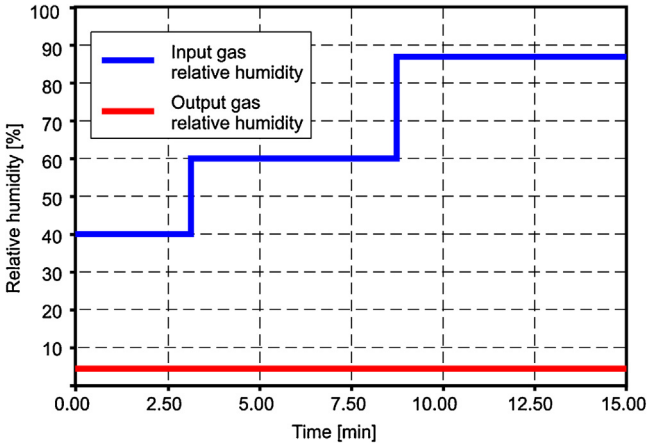

Fig. 21. Concentration of water was reduced to about 3%.

The described LAS systems were integrated into a measurement platform for the biomarkers detection (Fig. 20).

Breath sampling unit (BSU) and gas preparing unit (GPU) form the input blocks of the platform. The breath samples (either that one collected in tedlar bag or supplied directly by a breathing patient) are directed to the GPU, where water and aerosols concentrations are reduced by use of the coalescence particulate filter and nafion dryers. The filter eliminates the aerosols particles which diameters are larger than 0.1 μm. Nafion is able to reduce the water concentration about 30 times (Fig. 21). Input gas water vapour was prepared and controlled by KIN-TEK reference gas generator model 491M, output gas humidity was measured using E+E Elektronik humidity probe model EE07-MFT.

BSU is an independent, compact and portable device. Detailed information is given in our paper [77]. BSU can be functionally integrated with analyzers employing different detection methods (Fig. 22). Its main task is to select correct phase of the breath, where the concentration of the investigated biomarker is the highest. It can also provide easier identification of biomarker sources. To select

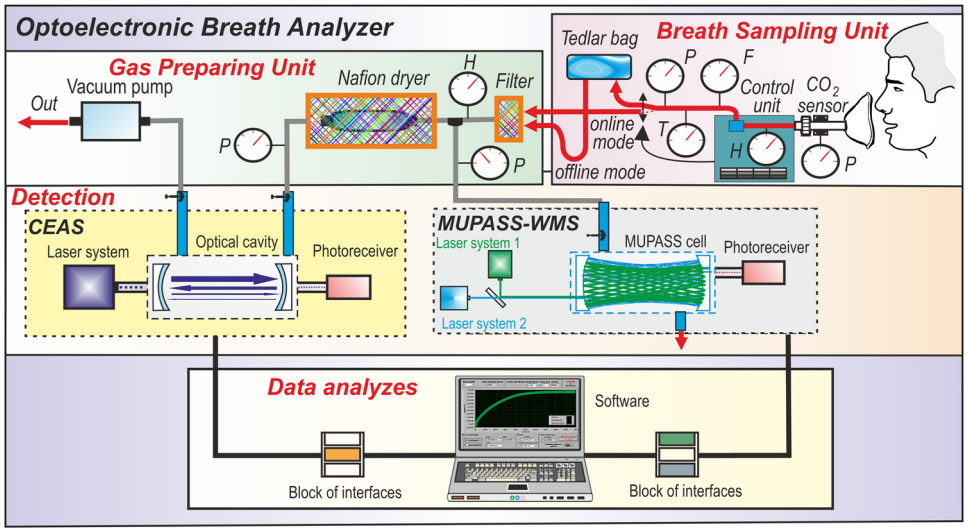

Fig. 20. Block diagram of the optoelectronic breath analyzer platform. P, T, H, F means pressure, temperature, humidity and flow sensors respectively.

Fig. 22. View of the BSU portable device during tests.

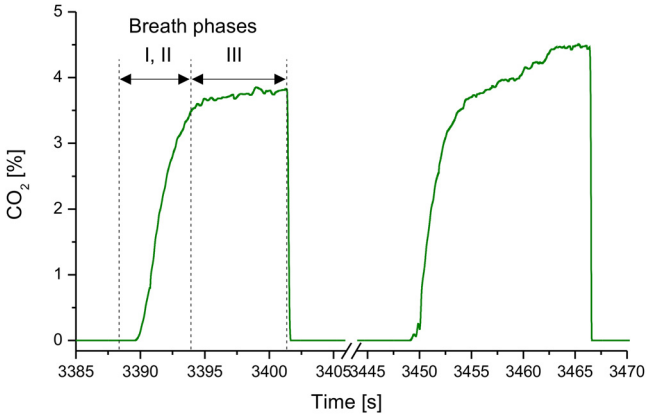

Fig. 24. Example of CO_2 concertation during patient breath collection.

proper breath phase non-dispersive infrared (NDIR) carbon dioxide (CO_2) commercial sensor model UT100C from UTECH capnograph unit was used. It performs continuous and real-time measurements (100 per second) of the exhaled CO_2 (ECO_2) in the concentration range of 0%–20% (0–150 mm Hg) with uncertainty 5% of reading. For proper patient's breath sample separation and collection, its pressure, temperature and humidity are measured as well. BSU also ensures patients protection against applying too high pressure from the synthetic air cylinder and to control synthetic air supply.

Construction of inhaled tubes allows delivering air to the patient in a proper way, without interruptions and in accordance with the respiratory cycle. Pressure of exhaled air sample is important because of needs of the exhaust cycle stabilization, maintaining pressure in a safe range (±20 mbar) and not overloading the patient. Humidity and temperature control is important for accurate biomarkers concentration measurements.

All sensors are handled by microcontroller system, which decides – using developed algorithm – about air sample circulation using a set of solenoid valves (*Ev*) (Fig. 23).

Three biomarker sensors (NO, CO and CH_4) and data analyzers are the next units of the platform. For CO and CH_4 detection, the application of MUPASS technique together with WMS was applied. The concentration measurements were performed by wavelength scanning within the range of 2.25366–2.2537 μm for CH_4 and 2.3360–2.33372 for CO. For this purpose, two single mode cw DFB-diode lasers were used. The half-meter sample cell composed of two metallic mirrors in White configuration was constructed. It provides 30 light reflections between the mirrors. Output beam is focused on a photodiode, which signal is demodulated with lock-in amplifier and averaged over 60 s. Good linear correlation between data supplied by the gas mixing system and the sensor was observed for both components within the concentration range of 0.4–100 ppm. The precision of the measurement was better than 0.1 ppm. That is sufficient for carbon monoxide and methane monitoring in human breath for both sick and healthy persons.

Nitric oxide CEAS sensor consists of a laser with the control system, optical cavity and photoreceiver. NO sensor provides sampling rate about 2 seconds.

The high detection performance of the sensor is obtained by matching DFB quantum cascade laser wavelength (Alpes Lasers SA) to the NO absorption wavelength, equal 5.2630 μm. Precise laser current driver and temperature controller (in laser control system) ensured high stability of generated wavelengths. The optical cavity was built of two concave dielectric mirrors, 60 cm apart, with effective optical path of radiation up to several hundred meters. Their reflectivity reached 0.995 at the wavelength of interest. The radiation from the cavity was registered with optimized detection modules PVI-4TE (VIGO System S.A.) [78]. The signal from the module was digitized and analyzed by data analysis subsystem. The detection limit of the sensor was about 30 ppb.

Example of real tests results of the BSU, GSU and NO sensor are presented in Figs. 24 and 25. Breath samples have been collected from patients suffering from various respiratory diseases. Despite very high CO_2 and H_2O concentrations in human breath, low fractional exhaled nitric (FeNO) concertation measurements were successfully performed. According American Thoracic Society (ATS) FeNO high limit for healthy adults is 50 ppb [79].

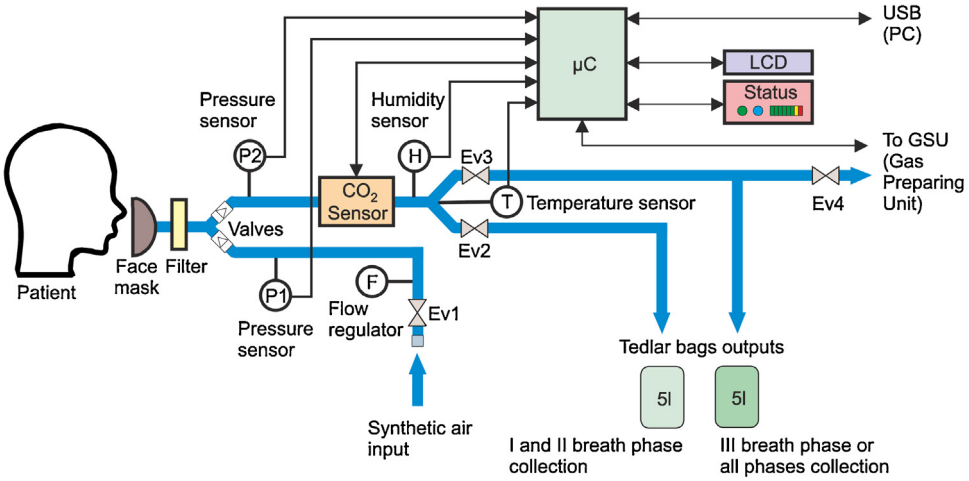

Fig. 23. Block diagram of the breath sampling unit.

Table 3
The test results of MUPASS and CEAS sensors.

Biomarker	Laser	Wavelength [μm]	Spectroscopic technique	Detection limit [ppb]
Ammonia	Diode laser DL 100, Toptica	1.527	MUPASS-WMS	1
Carbon monoxide	DFB-diode laser, Toptica	2.333	MUPASS-WMS	400
Carbon monoxide	OPG/DFG laser system type	4,783	CEAS	10
Carbonyl sulfide	PG711-DFG-SH, Ekspla	4.875	CEAS	1
Ethane		3.348	CEAS	3.5
Methane	DFB-diode laser, Toptica	2.253	MUPASS-WMS	100
Nitric oxide	QCL, Alpes Laser SA	5.262	CEAS	30
Nitrous oxide		4.53	CEAS	45
Carbonyl sulfide		5.257	CEAS	250

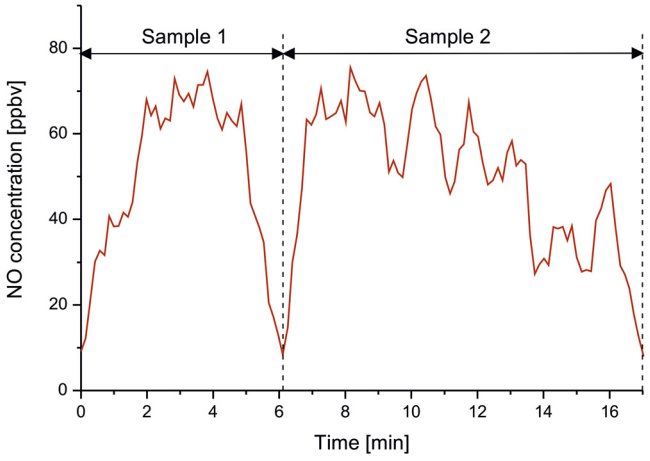

Fig. 25. Example of NO concentration measured in the sample collected in tedlar bag from phase III.

Authors has also developed LAS sensors capable to concentration measurements of ammonia, nitrous oxide, carbon monoxide and carbonyl sulfide. The detection limits are better than the maximal normal biomarker concentrations occurring in healthy man breath (Table 3).

5. Conclusions

Selected optoelectronic sensors for medical applications were presented. These devices can operate in invasive or non-invasive modes. The first group of the sensors includes: endoscopic imaging, bile sensor, pH meter, oxygen and carbon dioxide sensors, cardiac and pressure sensors. However, the most needed are the noncontact sensors that are able to perform the detection or the measurement procedures without physical contact with human body or the specimens such as blood, urine or other bodily fluids. Following examples of non-invasive instruments were described: pulse oximeter, blood flow-meter, glucose meter, sensor of prostate cancer, optical coherence tomography and human breath analyzers. Particular attention was paid to human breath analyzing that play increasing role in clinical diagnosis. Specific aspects of the applied methods are presented together with a discussion about their various implementations. The functionality of the system was obtained due to its construction consisting of four integrated units for breath collection, sample preparation, gas biomarkers detection and the data analyses. The required detecting parameters have been achieved due to application of two high-sensitive laser absorption spectroscopy methods. For the measurement of CH_4 and CO concentration two wavelength MUPASS-WMS sensor was constructed. The detection limits reached 100 ppb and 400 ppb, respectively. In the case of NO detection, the CEAS sensor with the detection limit of 30 ppb was applied. Real tests of the system with patients breath samples confirmed its great potential in medical diagnosis.

Acknowledgements

The research presented in this paper has been carried out in the laboratory of Institute of Optoelectronics MUT, supported by the National Centre for Research and Development and National Science Centre in the scope of Projects: ID: 179900, DEC-2011/03/B/ST7/02544.

References

[1] M.A. Perez, O. Gonzalez, J.R. Arias, Optical Fiber Sensors for Chemical and Biological Measurements, InTech, 2013, http://dx.doi.org/10.5772/52741 (Chapter 10).
[2] http://photobiology.info/Visser-Rolinski_files/Fig4.png.
[3] M. Mohamad, H. Manap, An overview of optical fibre sensors for medical applications, Int. J. Eng. Technol. Sci. 1 (2014) 9–11.
[4] L.M. Lechuga, A. Calle, F. Prieto, Optical sensor based on evanescent field sensing. Part I: surface plasmon resonance sensors, Anal. Chem. 19 (Suppl) (2000) 54–60.
[5] S. Silvestri, E. Schena, Optical-Fiber Measurement Systems for Medical Application, InTech, 2013, http://dx.doi.org/10.5772/18845 (Chapter 11).
[6] A. Mendez, Medical Applications of Fiber-Optics: Optical Fibers Sees Growth as Medical Sensors, Laser Focus World, 2011, 01/01.
[7] H.W. Dremel, General principles of endoscopic imaging, in: A. Ernst, F.J.F. Herth (Eds.), Principles and Practice of Interventional Pulmonology, vol. 15, Springer Science+Business Media, New York, 2013.
[8] F. Baldini, Invasive sensors in medicine, in: NATO SCI SER II MATH, Springer, 2006, pp. 417–435.
[9] http://www.cecchi.com/apparecchi-medicali/.
[10] R. Falciai, A.M. Scheggi, F. Baldini, P. Bechi, Method of Detecting Enterogastric Reflux and Apparatus for the Implementation of This Method, European Patent number 0323816B1 6-11-91.
[11] P. Bechi, R. Falciai, F. Baldini, F. Cosi, F. Pucciani, S. Boscherini, New fiber optic sensor for ambulatory entero-gastric reflux detection, Proceedings P SOC PHOTO-OPT INS vol. 1648 (1992), http://dx.doi.org/10.1117/12.58293.
[12] O.S. Wolfbeis, Fiber Optic Chemical Sensors and Biosensors, CRC Press, Boca Raton, 1991.
[13] I. Kasik, J. Mrazek, T. Martan, et al., Fiber-optic pH detection in small volumes of biosample, Anal. Bioanal. Chem. 398 (5) (2010) 1883–1889.
[14] Y. Xiong, Y. Huang, Z. Ye, Y. Guan, Flow injection small volume fiber-optic pH sensor based on evanescent wave excitation and fluorescence determination, J. Fluoresc. 21 (3) (2011) 1137–1142.
[15] D. Wencel, T. Abel, C. McDonagh, Optical chemical pH sensors, Anal. Chem. 86 (1) (2014) 15–29.
[16] P. Baldini, S. Bechi, F. Bracci, In vivo optical-fibre sensor for gastro-oesophageal measurement, Sens. Actuators B 29 (1995) 164–168.
[17] Technical Compedium CDI Blood Parameter Monitoring System 500, 2017.
[18] http://www.terumo-cvgroup.com/_video/858768_CDI500-VIDEO_DEC2015_FINAL.shtml.
[19] J.A.C. Heijmans, L.K. Cheng, F.P. Wieringa, Optical fiber sensors for medical application – practical engineering considerations, IFMBE Proc. 22 (2008) 2330–2334.
[20] P. Rolfe, F. Scopesi, G. Serra, Advances in fiber-optic sensing in medicine and biology, Meas. Sci. Technol. 18 (6) (2007) 1683–1688.
[21] G. Konieczny, Z. Opilski, T. Pustelny, E. Maciak, State of the work diagram of the artificial heart, Acta Phys. Pol. 116 (September (3)) (2009).
[22] G. Konieczny, Z. Opilski, T. Pustelny, A. Gacek, et al., Results of experiments with fiber pressure sensor applied in the polish artificial heart prosthesis, Acta Phys. Pol. A 118 (6) (2010) 1182–1184.
[23] Y. Lochner, A. Khan, All-organic optoelectronic sensor for pulse oximetry, Nat. Commun. (2014) www.nature.com/naturecommunications.
[24] I. Fredriksson, C. Fors, J. Johansson, Laser Doppler Flowmetry – A Theoretical Framework, Department of Biomedical Engineering, Linköping University, 2007 www.imt.liu.se/bit/ldf/ldfmain.html.
[25] H. Jafarzadeh, Laser Doppler flowmetry in endodontics: a review, Int. Endod. J. 42 (2009) 476–490.

[26] H.E. Albrecht, N. Damaschke, M. Borys, C. Tropea, Laser Doppler and Phase Doppler Measurement Techniques, Springer, New York, 2003, pp. 4–30.
[27] Y. Kimura, P. Wilder-Smith, K. Matsumoto, Lasers in endodontics: a review, Int. Endod. J. 33 (2000) 173–185.
[28] J. Kottmann, U. Grob, J.M. Rey, M.W. Sigrist, Mid-Infrared fiber-coupled photoacoustic sensor for biomedical applications, Sensors 13 (2013) 535–549.
[29] A. Ergin, G.A. Thomas, Non-invasive detection of glucose in porcine eyes, Bioengineering Conference, Proc. IEEE 31st Annual Northeast (2005).
[30] http://www.microspectra.com/support/the-science/raman-science.
[31] C. Camerlingo, I. Delfino, G. Perna, V. Capozzi, M. Lepore, Micro-Raman spectroscopy and univariate analysis for monitoring disease follow-up, Sensors 11 (2011) 8309–8322.
[32] M. Gnyba, M.S. Wróbel, K. Karpienko, D. Milewska, M. Jędrzejewska-Szczerska, Combined analysis of whole human blood parameters by Raman spectroscopy and spectral-domain low-coherence interferometry, in: Proc. SPIE 9537, Clinical and Biomedical Spectroscopy and Imaging IV, 15 July, 2015, http://dx.doi.org/10.1117/12.2183645, 95371N.
[33] J.M. Smulko, N.C. Dingari, J.S. Soares, I. Barman, Anatomy of noise in quantitative biological Raman spectroscopy, Bioanalysis 6 (2014) 411–421.
[34] M. Wróbel, M. Gnyba, M. Jedrzejewska-Szczerska, T. Myllyla, J. Smulko, I. Barman, Sensing of anesthetic drugs in blood with Raman spectroscopy, in: Advanced Photonics 2015, Optical Society of America, 2015, OSA Technical Digest (online), paper SeS1B.4.
[35] G.H. Wu, R.H. Datar, K.M. Hansen, T. Thundat, R.J. Cote, A. Majumdar, Bioassay of prostatespecific antigen (PSA) using microcantilever, Nat. Biotechnol. 19 (2001) 85660.
[36] https://www.nae.edu/20683.aspx.
[37] B. Povazay, K. Bizheva, A.H. Unterhuber, B. Hermann, H. Sattmann, A.F. Fercher, W. Drexler, A. Apolonski, et al., Submicrometer axial resolution optical coherence tomography, Opt. Lett. 27 (2002) 1800.
[38] A. Szkulmowska, M. Szkulmowski, A. Kowalczyk, M. Wojtkowski, Retinal blood flow analysis using spectral OCT: joint spectral and time domain OCT versus phase-resolved Doppler OCT, Invest. Ophthalmol. Vis. Sci. 49 (2008), 1873–1873.
[39] A.M. Rollins, R. Ung-arunyawee, A. Chak, R.C.K. Wong, K. Kobayashi, M.V. Sivak, J.A. Izatt, Real-time in vivo imaging of human gastrointestinal ultrastructure by use of endoscopic optical coherence tomography with a novel efficient interferometer design, Opt. Lett. 24 (1999) 1358–1360.
[40] J.A. Izatt, M.D. Kulkarni, S. Yazdanfar, J.K. Barton, A.J. Welch, In vivo bi-directional color Doppler flow imaging of picoliter blood volumes using optical coherence tomography, Opt. Lett. 22 (1997) 4139–4141.
[41] M. Wojtkowski, A. Kowalczyk, R. Leitgeb, A.F. Fercher, Complex spectral OCT in eye imaging, Opt. Lett 27 (16) (2002) 1415–1417.
[42] S. Tamborski, H.C. Lyu, H. Dolezyczek, M. Malinowska, G. Wilczynski, D. Szlag, T. Lasser, M. Wojtkowski, M. Szkulmowski, Extended-focus optical coherence microscopy for high-resolution imaging of the murine brain, Biomed. Opt. Express 7 (11) (2016) 4400–4414.
[43] K. Karnowski, A. Ajduk, B. Wieloch, S. Tamborski, K. Krawiec, M. Wojtkowski, M. Szkulmowski, Optical coherence microscopy as a novel, non-invasive method for the 4D live imaging of early mammalian embryos, Sci. Rep. 7 (1) (2017) 4165, http://dx.doi.org/10.1038/s41598-017-04220-8.
[44] R. Leitgeb, M. Wojtkowski, C.K. Hitzenberger, M. Sticker, A. Kowalczyk, A.F. Fercher, Spectral measurement of absorption by spectroscopic frequency-domain OCT, Opt. Lett. 25 (2000) 820–822.
[45] Y. Zahid, J. Wu, Ch. Yang, Spectral domain optical coherence tomography: a better OCT imaging strategy, BioTechniques 39 (December) (2005) S6–S13, http://dx.doi.org/10.2144/000112090.
[46] A. Ulanowska, T. Ligor, M. Michel, B. Buszewski, Hyphenated and unconventional methods for searching volatile cancer biomarkers, Ecol. Chem. Eng. 17 (1) (2010) 9–23.
[47] B. Buszewski, D. Grzywinski, T. Ligor, T. Stacewicz, Z. Bielecki, J. Wojtas, Detection of volatile organic compounds as biomarkers in breath analysis by different analytical techniques, Bioanalysis 5 (18) (2013) 2287–2306.
[48] P.J. Mazzone, Exhaled breath volatile organic compound biomarkers in lung cancer, J. Breath Res. 6 (2012) 027106.
[49] A. Ulanowska, E. Trawinska, P. Sawrycki, B. Buszewski, Chemotherapy control by breath profile with application of SPME-GC/MS method, J. Sep. Sci. 35 (2012) 2908–2913.
[50] I.B. Silva, A.C. Freitas, T.A.P. Rocha-Santos, M.E. Pereira, A.C. Duarte, Breath analysis by optical fiber sensor for the determination of exhaled organic compounds with a view to diagnostics, Talanta 83 (2011) 1586–1594.
[51] S. Kumar, J. Huang, J.R. Cushnir, P. Spanel, D. Smith, G.B. Hanna, Selected ion flow tube-ms analysis of headspace vaper from gastric content for the diagnosis of gastro-esophageal cancer, Anal. Chem. 84 (2012) 9550–9557.
[52] E.H. Oh, H.S. Song, T.H. Park, Recent advances in electronic and bioelectronic noses and their biomedical applications, Enzyme Microb. Technol. 48 (6–7) (2011) 427–437.
[53] T. Stacewicz, J. Wojtas, Z. Bielecki, M. Nowakowski, J. Mikolajczyk, R. Medrzycki, B. Rutecka, Cavity ring down spectroscopy: detection of trace amounts of matter, Opto-Electron. Rev. 20 (2012) 34–41.
[54] K. Musa-Veloso, S.S. Likhodii, E. Rarama, S. Benoit, Y.M.C. Liu, D. Chartrand, R. Curtis, L. Carmant, A. Lortie, F.J.E. Comeau, S.C. Cunnane, Breath acetone predicts plasma ketone bodies in children with epilepsy on a ketogenic diet, Nutrition 22 (2006) 1–8.
[55] J.C. Anderson, W.J.E. Lamm, M.P. Hlasatala, Measuring airway exchange of endogenous acetone using a single-exhalation breathing maneuver, J. Appl. Physiol. 100 (2005) 880–889.
[56] C.J. Wang, S.T. Scherrer, D. Hossain, Measurements of cavity ringdown spectroscopy of acetone in the ultraviolet and near infrared spectral regions: potential for development of a breath analyzer, Appl. Spectrosc. 58 (7) (2004) 784–791.
[57] D.J. Kearney, T. Hubbard, D. Putnam, Breath ammonia measurement in Helicobacter pylori infection, Dig. Dis. Sci. 47 (2002) 2523–2530.
[58] D. Smith, T. Wang, A. Pysanenko, P. Spanel, A selected ion flow tube mass spectrometry study of ammonia in mouth- and nose-exhaled breath and in the oral cavity, Rapid Commun. Mass Spectrom. 22 (2008) 783–789.
[59] D.K. Stevenson, H.J. Vreman, Carbon monoxide and bilirubin production in neonates, Pediatr. Rev. 100 (1997) 252–259.
[60] M. Yamaya, K. Sekizawa, S. Ishizuka, M. Monma, K. Mizuta, H. Sasaki, Increased carbon monoxide in exhaled air of subjects with upper respiratory tract infections, Am. J. Respir. Crit. Care Med. 158 (1998) 311–314.
[61] M.J. Thorpe, K.D. Moll, J.R. Jones, B. Safdi, J. Ye, Broadband cavity ringdown spectroscopy for sensitive and rapid molecular detection, Science 311 (2006) 1595–1599.
[62] G. Neri, A. Bonavita, S. Ipsale, G. Micali, G. Rizzo, N. Donato, Carbonyl Sulphide (COS) monitoring on MOS sensors for biomedical applications, ISIE 2007 (2007) 2776–2781.
[63] L. Bennett, L. Ciaffoni, W. Denzer, G. Hancock, A.D. Lunn, R. Peverall, S. Praun, G.A.D. Ritchie, A chemometric study on human breath mass spectra for biomarker identification in cystic fibrosis, J. Breath Res. 3 (2009) 1–7.
[64] C. Fischer, M.W. Sigrist, Trace gas sensing in the 3.3 μm region using a diode based difference frequency laser photoacoustic system, Appl. Phys. B: Lasers Opt. 75 (2002) 305–310.
[65] S.R. Svedahl, K. Svendsen, E. Tufvesson, P.R. Romundstad, A.K. Sjaastad, T. Qvenild, B. Hilt, Inflammatory markers in blood and exhaled air after short-term exposure to cooking fumes, Ann. Occup. Hyg. 57 (2) (2012) 230–239.
[66] R. Matthew, Y.B. McCurdy, G. Wysocki, R. Lewicki, F.K. Tittel, Recent advances of laser-spectroscopy-based techniques for applications in breath analysis, J. Breath Res. 1 (2007) 014001.
[67] G.D. Lawrence, G. Cohen, Ethane exhalation as an index of in vivo lipid peroxidation: concentrating ethane from a breath collection chamber, Anal. Biochem. 122 (1982) 283–290.
[68] C.S. Patterson, L.C. McMillan, K. Stevenson, K. Radhakrishnan, P.G. Shiels, M.J. Padgett, K.D. Skeldon, Dynamic study of oxidative stress in renal dialysis patients based on breath ethane measured by optical spectroscopy, J. Breath Res. 1 (2) (2007) 026005:1–026005:8.
[69] W. Miekisch, J.K. Schubert, G.F. Noeldge-Schomburg, Diagnostic potential of breath analysis-focus on volatile organic compounds, Clin. Chim. Acta 347 (2004) 25–39, http://dx.doi.org/10.1016/j.cccn.2004.04.023.
[70] L. Le Marchand, L.R. Wilkens, P. Harwood, R.V. Cooney, Use of breath hydrogen and methane as markers of colonic fermentation in epidemiologic studies: circadian patterns of excretion, Environ. Health Perspect. 98 (1992) 199–202.
[71] K. McCluskie, M.A. Birrell, S. Wong, M.G. Belvisi, Nitric oxide as a noninvasive biomarker of lipopolysaccharide-induced airway inflammation: possible role in lung neutrophilia, J. Pharmacol. Exp. Ther. 311 (2004) 625–633.
[72] M.A. Birrell, K. McCluskie, E. Hardaker, R. Knowles, M.G. Belvisi, Utility of exhaled nitric oxide as a noninvasive biomarker of lung inflammation in a disease model, Eur. Respir. J. 28 (2006) 1236–1244.
[73] http://www.thoracic.org/about/overview.php.
[74] T. Kondo, T. Mitsui, M. Kitagawa, Y. Nakae, Association of fasting breath nitrous oxide concentration with gastricjuice nitrate and nitrite concentrations and helicobacter pylori infection, Dig. Dis. Sci. 45 (2000) 2054–2057.
[75] R.A. Dweik, D. Laskowski, H.M. Abu-Soud, F.T. Kaneko, R. Hutte, D.J. Stuehr, S.C. Erzurum, Nitric oxide synthesis in the lung, regulation by oxygen through a kinetic mechanism, J. Clin. Invest. 101 (1998) 660–666.
[76] Y. Wang, M. Nikodem, E. Zhang, F. Cikach, J. Barnes, S. Comhair, R. Dweik, C. Kao, G. Wysocki, Shot-noise limited Faraday rotation spectroscopy for detection of nitric oxide isotopes in breath, urine, and blood, Sci. Rep. 5 (2015), http://dx.doi.org/10.1038/srep09096, Article 9096.
[77] D. Szabra, A. Prokopiuk, J. Mikołajczyk, T. Ligor, B. Buszewski, Z. Bielecki, Air sampling unit for breath analyzers, Rev. Sci. Instrum. 88 (2017), 115006-1–115006-6.
[78] https://www.vigo.com.pl/.
[79] American Thoracic Society, European Respiratory Society, ATS/ERS recommendations for standardized procedures for the online and offline measurement of exhaled lower respiratory nitric oxide and nasal nitric oxide, Am. J. Respir. Crit. Care Med. 171 (2005) 912–930.